Progress in Flight Dynamics, GNC, and Avionics **6** (2013) 685-706
DOI: 10.1051/eucass/201306685

AN $\mathcal{H}_\infty$ FULL INFORMATION APPROACH FOR THE FEEDFORWARD CONTROLLER DESIGN OF A LARGE BLENDED WING BODY FLEXIBLE AIRCRAFT

C. Westermayer, A. Schirrer, M. Hemedi, and M. Kozek

Institute of Mechanics and Mechatronics
Vienna University of Technology
8 Wiedner Hauptstr., Vienna 1040, Austria

An $\mathcal{H}_\infty$ full information feedforward design approach for longitudinal motion prefilter design of a large flexible blended wing body (BWB) aircraft is presented. An existing onset is extended such that specifications concerning command tracking, limited control energy, and manoeuvre load reduction can be addressed simultaneously. Therefore, the utilized design architecture is provided and manual tuning aspects are considered. In order to increase controller tuning efficiency, an automated tuning process based on several optimization criteria is proposed. Moreover, two design methodologies for the parameter-varying design case are investigated. The obtained controller is validated on a high-order nonlinear model, indicating the high potential of the presented approach for flexible aircraft control.

1 INTRODUCTION

Control of flexible aircraft is a research topic of high interest [1–5], since it represents a challenging control design application pursuing the primary goal of reduced structural weight. This, in turn, means increased fuel efficiency, which is also expected by utilization of BWB configurations. The control design of just such a flexible BWB configuration is considered in this paper. It is a challenging task, because on the one hand, many design requirements have to be considered at the same time. On the other hand, these requirements have to be fulfilled for a large flight envelope and additional parameters which vary strongly. Moreover, the design models are of high order due to the considered aeroelasticity, which, in turn, drives modern control design methodologies into computational limits.

The design of robust $\mathcal{H}_\infty$ controllers using μ-synthesis is presented in [1]. First, the modeling process for combined flight mechanic and aeroelastic modeling for a large four engine aircraft is outlined, followed by the separated controller design process for longitudinal and lateral motion. The obtained results concerning rigid-body dynamic control and flexible mode damping justify the chosen approach.

An *a priori* self-scheduling control approach for the longitudinal motion of a flexible aircraft is shown in [6]. There, the convex synthesis design methodology is applied on a linear fractional transformation (LFT) model. The performance specifications are implemented by shaping the closed-loop transfer functions utilizing a parameterized observer and Youla-parameter.

Two further convex synthesis approaches for lateral control of a BWB type flexible aircraft are presented in [7, 8]. In [8], the focus is on a robust multiobjective feedback design, considering both time- and frequency-domain specifications. Thereby, significant reductions of loads and vibrations are obtained. In [7], a multimodel feedforward design approach is shown. Design specifications concerning manoeuvre load reduction and command tracking are addressed.

In [9], a linear parameter-varying (LPV) design approach for the longitudinal motion of a BWB type aircraft is presented. The utilized method is based on parameter-dependent Lyapunov functions. Design specifications concerning handling qualities, loads, and vibration damping are addressed for varying Mach number.

From the aforementioned references, it becomes evident that typical design goals of flexible aircraft control are (i) robust stabilization; (ii) correct pole placement; (iii) reduction of loads caused by turbulence and gust; $(i\nu)$ vibration damping; (ν) correct command response; and (νi) maneuver load reduction. Considering all design goals at once leads to an extremely complex design and makes controller tuning tedious and difficult. A typical approach is given by a separation of the controller design in a feedback $\boldsymbol{K}_{\mathrm{fb}}$ and a feedforward $\boldsymbol{K}_{\mathrm{ff}}$ part representing together a two degree of freedom (2DOF) concept (Fig. 1), where $\boldsymbol{K}_{\mathrm{fb}}$ is responsible for design goals (i) to $(i\nu)$ while $\boldsymbol{K}_{\mathrm{ff}}$ has to accomplish goals (ν) and (νi).

In this paper, the focus lies on the design of the feedforward part using an $\mathcal{H}_\infty$ full information approach [10], where the feedforward design is fully decoupled

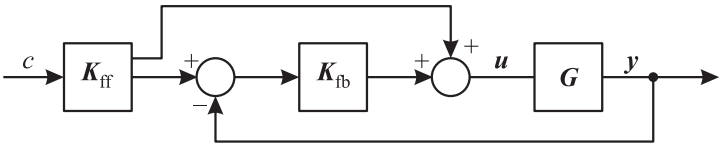

Figure 1 General 2DOF control configuration

from the feedback design. Thereby, the main contribution of this work is the extension of the approach in [10] such that it can be utilized for manoeuvre load control. Applied to a flexible BWB aircraft, several design specifications have to be considered at once over a large flight envelope, which makes the use of a parameter scheduling onset inevitable. The contents of the paper are structured as follows. First, the BWB model is introduced and a problem formulation given. Then, the design methodology is presented, followed by a controller tuning process. In the next section, an extension from nominal to LPV and gain-scheduled design, respectively, is presented. Finally, the obtained validation results from nonlinear simulations are presented and the positive outcomes concerning tracking and manoeuvre load reduction over a large flight envelope are discussed.

2 SYSTEM MODEL

The system model is an integrated model of a large two-engine BWB passenger aircraft as shown in Fig. 2, i. e., the model contains flight mechanics, aeroelastics, and their coupling [12, 13]. For various Mach numbers Ma, dynamic pressure conditions q, fuel-mass cases f, and center of gravity positions CG, the nonlinear system is linearized in trimmed cruise conditions. The decoupling of longitudinal and lateral dynamics is utilized in this work to focus on the longitudinal motion only. Due to the utilized modeling methodologies based on computational fluid dynamics (CFD) and finite element (FE) methods, the original linearized models

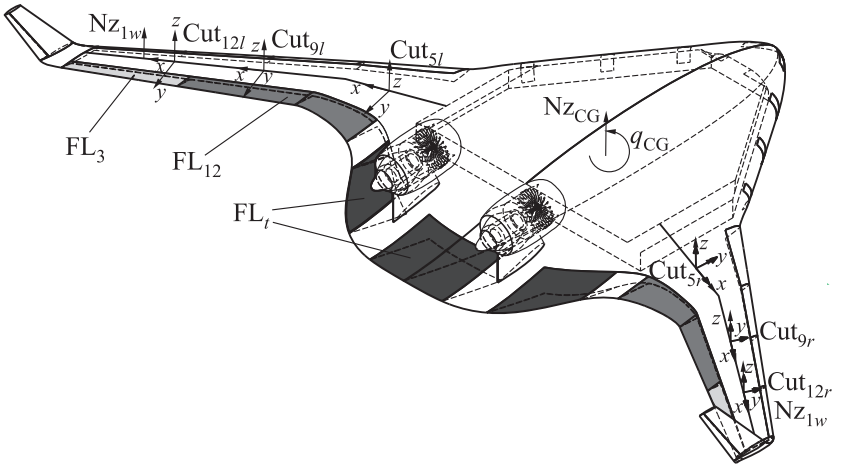

Figure 2 Schematic sketch of BWB aircraft with relevant system inputs and outputs [11]

are of high order, making their use for control design infeasible. Therefore, those models are reduced by adequate reduction techniques to comparatively low-order design models containing only the most important flexible modes [13]. The reduced models $\boldsymbol{G}$ are given in state space representation

$$\begin{bmatrix} \dot{\boldsymbol{x}}(t) \\ \boldsymbol{e}(t) \\ \boldsymbol{y}(t) \end{bmatrix} = \underbrace{\begin{bmatrix} \boldsymbol{A} & \boldsymbol{B}_d & \boldsymbol{B}_u \\ \boldsymbol{C}_e & \boldsymbol{D}_{11} & \boldsymbol{D}_{12} \\ \boldsymbol{C}_y & \boldsymbol{D}_{21} & \boldsymbol{D}_{22} \end{bmatrix}}_{\boldsymbol{G}} \begin{bmatrix} \boldsymbol{x}(t) \\ \boldsymbol{d}(t) \\ \boldsymbol{u}(t) \end{bmatrix} \tag{1}$$

with the corresponding state vector

$$\boldsymbol{x} = \begin{bmatrix} w \; q \; \xi_1 \; \dot{\xi}_1 \; \cdots \; \xi_s \; \dot{\xi}_s \; x_{l_1} \; \cdots \; x_{l_t} \end{bmatrix}^{\mathrm{T}}$$

where w is the vertical velocity; q is the pitch rate (together forming the short period mode); ξ_j and $\dot{\xi}_j$ $(j = 1, \ldots, s)$ are the modal deflection and modal deflection rate of the aeroelastic modes, respectively; and x_{l_k} $(k = 1, \ldots, t)$ are the lag states. The validation model used in section 6 has $s = 19$ aeroelastic modes and $t = 14$ lag states. The design methodology based on the linear matrix inequalities (LMIs) presented in this work requires a model of reduced complexity. Therefore, the design model contains only the first and second wing bending mode ($s = 2$) and $t = 4$ lag states. While for the exogenous input to system (1) $\boldsymbol{d} = 0$ holds, the control input vector is given by

$$\boldsymbol{u} = \begin{bmatrix} \delta_{\mathrm{EL}_t} \; \dot{\delta}_{\mathrm{EL}_t} \; \delta_{\mathrm{FL}_{12}} \; \dot{\delta}_{\mathrm{FL}_{12}} \; \delta_{\mathrm{FL}_3} \; \dot{\delta}_{\mathrm{FL}_3} \end{bmatrix}^{\mathrm{T}} \tag{2}$$

where δ_i and $\dot{\delta}_i$ are the deflection and deflection rate, respectively, of the combined elevator EL_t, the combined inner flap FL_{12}, and the outer flap FL_3. The measurement vector $\boldsymbol{y}$ contains the three measurements utilized by the corresponding LPV feedback controller of the 2DOF concept:

$$\boldsymbol{y} = \begin{bmatrix} \mathrm{Nz}_{\mathrm{CG}} \; q_{\mathrm{CG}} \; \mathrm{Nz}_{\mathrm{law}} \end{bmatrix}^{\mathrm{T}} \tag{3}$$

where $\mathrm{Nz}_{\mathrm{law}}$ is the modal wing bending acceleration signal used to separate the vertical wing bending from the rigid body motion:

$$\mathrm{Nz}_{\mathrm{low}} = \frac{\mathrm{Nz}_{\mathrm{lw}} + \mathrm{Nz}_{\mathrm{rw}}}{2} - \mathrm{Nz}_{\mathrm{CG}}$$

The exogenous output vector $\boldsymbol{e}$ is given by three load outputs:

$$\boldsymbol{e} = \begin{bmatrix} \mathrm{My}_5 \; \mathrm{My}_9 \; \mathrm{My}_{12} \end{bmatrix}^{\mathrm{T}} \tag{4}$$

where My_i represent the cut bending moments along the wing. While for the design only three cut moments are selected, a more closely spaced grid of cut moments and also cut forces Fz_i is considered for controller validation in section 6.

In order to obtain the final model $\boldsymbol{G}_{\mathrm{ff}}$ for design and validation, the open-loop system $\boldsymbol{G}$ has to be augmented by actuator and sensor dynamics:

$$\boldsymbol{G}_{\mathrm{ff}} = \boldsymbol{G}_{\mathrm{sen}}\ \boldsymbol{G}\ \boldsymbol{G}_{\mathrm{act}}\,. \tag{5}$$

Therefore, nonlinear actuator models depending on the dynamic pressure q are linearized and reduced to second-order low-pass filters:

$$\boldsymbol{G}_{\mathrm{act}} = \begin{bmatrix} \dfrac{7.5}{s^2+3.9s+7.5} & 0 & 0 \\ \dfrac{7.5s}{s^2+3.9s+7.5} & 0 & 0 \\ 0 & \dfrac{19.7}{s^2+6.3s+19.7} & 0 \\ 0 & \dfrac{19.7s}{s^2+6.3s+19.7} & 0 \\ 0 & 0 & \dfrac{60.7s}{s^2+11.0s+60.7} \\ 0 & 0 & \dfrac{60.7s}{s^2+11.0s+60.7} \end{bmatrix}.$$

The sensor delays are modeled by first-order Padé approximations and Butterworth filters are approximated by PT1 elements:

$$\boldsymbol{G}_{\mathrm{sen}} = \begin{bmatrix} \dfrac{-15(s-12.5)}{(s+15)(s+12.5)} & 0 & 0 & 0\,0\,0 \\ 0 & \dfrac{-15(s-12.5)}{(s+15)(s+12.5)} & 0 & 0\,0\,0 \\ 0 & 0 & \dfrac{-(s-33.3)}{s+33.3} & 0\,0\,0 \\ 0 & 0 & 0 & 1\,0\,0 \\ 0 & 0 & 0 & 0\,1\,0 \\ 0 & 0 & 0 & 0\,0\,1 \end{bmatrix}.$$

Due to the additional actuator dynamics, the input vector (2) is replaced by

$$\boldsymbol{u} = \left[\, \eta_{\mathrm{EL}_t}\ \eta_{\mathrm{FL}_{12}}\ \eta_{\mathrm{FL}_3} \,\right]^{\mathrm{T}} \tag{6}$$

where η_i, $i \in \{\mathrm{EL}_t, \mathrm{FL}_{12}, \mathrm{FL}_3\}$ is the respective actuator deflection command.

As already mentioned above, the system is linearized for the flight parameters Ma and q and for the additional parameters f and CG, which together span the

flight envelope. While the CG parameter is kept constant for the following considerations, the remaining parameters can vary in the following range:

$$0.82 \leq \mathrm{Ma} \leq 0.88\,; \quad 8\,000\ \mathrm{Pa} \leq q \leq 17\,238\ \mathrm{Pa}\,; \quad 0\% \leq f \leq 100\%\,. \tag{7}$$

2.1 Open Loop Analysis

In the following, a short open-loop analysis of the system dynamics for varying fuel mass and a chosen cruise case is presented. The second-order longitudinal rigid body dynamic is represented by the short period mode (SPM), which is a conjugate complex pole pair for low fuel mass cases as shown in Fig. 3*a*. With increasing fuel mass, the SPM forms two real poles, where one of them becomes unstable while the second moves towards the left. In this pole zero map, also, the combined elevator (EL_t) pole is visible with a frequency of about $\omega = 2.8$ rad/s and a damping of $\zeta = 0.7$. The first symmetric flexible mode, representing the first wing bending mode, has a natural frequency between 9.8 and 10.9 rad/s and a minimum damping of $\zeta = 0.058$. The minimum frequency of the second flexible mode is 20.5 rad/s, while the damping is $\zeta = 0.017$. In Fig. 3*b*, the sigma plot from the combined elevator EL_t to $\mathrm{Nz_{CG}}$ is shown. In the low-frequency region, strong variations in the DC-gain are visible while above 20 rad/s, some flexible modes can be seen.

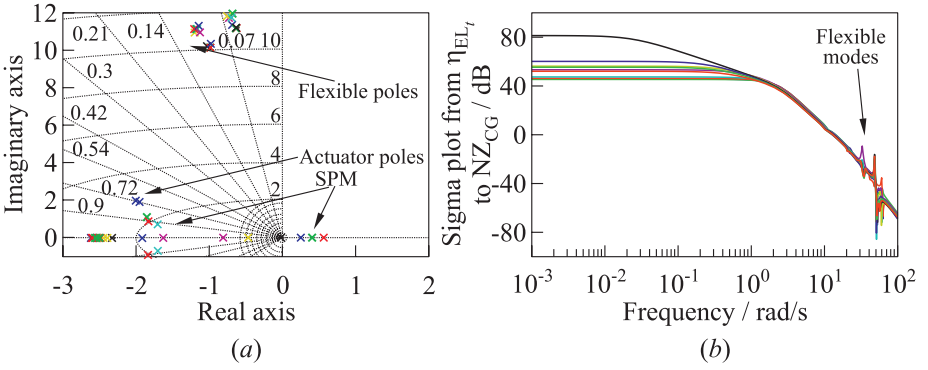

Figure 3 Pole zero map of the open-loop aircraft for varying fuel mass (*a*); and sigma plot from η_{EL_t} to $\mathrm{Nz_{CG}}$ for varying fuel mass (*b*).

2.2 Problem Definition

The design specifications to be addressed in the controller design process are given as follows:

(1) $\mathrm{Nz_{CG}}$ reference command response with a settling time between 3 and 5 s without overshoot. For the corresponding q_{CG} response, a maximum overshoot of 30% is tolerated;

(2) limitation of actuator deflection and deflection rate in order to avoid exceeding the existing saturation and rate limits; and

(3) reduction of structural loads represented by cut moments My_i and cut forces Fz_i along the wing.

All these specifications have to be fulfilled over the considered flight envelope according to (7). The performance of designed controllers has to be demonstrated together with an appropriate feedback control law on a high-order validation model including nonlinear actuator dynamics and corresponding rate and saturation limits.

3 DESIGN METHODOLOGY

The methodology considered in this paper is based on the findings in [10] where a full information approach is presented for the design of the feedforward part of a 2DOF controller. Related topics are found in [14, 15]. The approach is based on the fact that the design of the feedback part (the regulator) is completely decoupled from the design of the feedforward part (the prefilter). This means that the feedforward filter represents an extension to an existing closed loop as shown in Fig. 4 where the 2DOF control architecture for the given problem is presented. The control signals from $\boldsymbol{K}_{\mathrm{fb}}$ and $\boldsymbol{K}_{\mathrm{ff}}$ are summed up forming the combined control signal $\boldsymbol{u}_{\mathrm{c}}$. As indicated in this figure, $\boldsymbol{K}_{\mathrm{fb}}$ has two outputs, the combined elevator η_{EL_t} and the outer flap η_{FL_3}; $\boldsymbol{K}_{\mathrm{ff}}$ has an additional output, the combined inner flap $\eta_{\mathrm{FL}_{12}}$. The inputs to $\boldsymbol{K}_{\mathrm{fb}}$ are not the measurements $\mathrm{Nz_{CG}}$, q_{CG}, and $\mathrm{Nz_{law}}$ directly, but instead, its deviations from the ideal system response generated by $\boldsymbol{K}_{\mathrm{ff}}$. The full information feedforward controller is a prefilter, which has no direct influence on the stability of the closed loop system, as far as the demanded control inputs stay within the maximum deflection and

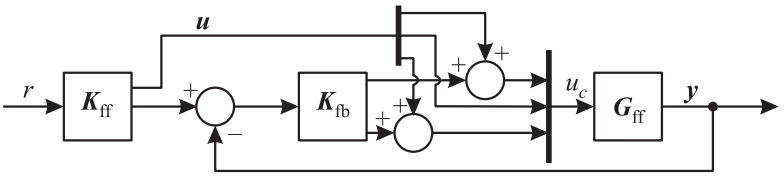

Figure 4 Specific 2DOF architecture: $z = \mathrm{Nz_{CGc}}$; $\boldsymbol{u}$ is defined in (6); and $\boldsymbol{y}$ in (3)

deflection rate limits. Thus, stability is not a primary issue of the design. On the contrary, tracking performance strongly depends on the model accuracy. Deviations of the design model from the real system have to be compensated by $\boldsymbol{K}_{\mathrm{fb}}$. Therefore, validation results are obtained from simulations of the complete system setup (see Fig. 4) where an LPV feedback controller similar to the one designed in [9] is utilized.

3.1 Design Architecture

The first step of the $\mathcal{H}_\infty$ full information feedforward design process is to define an appropriate design architecture representing a standard problem formulation in the $\mathcal{H}_\infty$ framework [16]. The augmented plant used in this work, which addresses the essential design specifications, is shown in Fig. 5. It represents a model matching problem, which means that a desired system time response is determined due to an appropriate reference model T_{ref} and the difference between the open loop model $\boldsymbol{G}_{\mathrm{ff}}$ and the reference model has to be minimized using the performance weight $\boldsymbol{W}_y$. The only output to be tracked here is the $\mathrm{Nz_{CG}}$ measurement. Moreover, two additional performance outputs $\boldsymbol{z}_u$ and $\boldsymbol{z}_p$ are defined in order to address specifications concerning limited control energy and manoeuvre load control. The latter performance output $\boldsymbol{z}_p$ represents an extension to the approach in [10]. As indicated by a double arrow, the first input vector to the static feedback matrix $\boldsymbol{F}$ is the completely available state vector of the augmented plant $\boldsymbol{P}$. Together with the reference input signal r, they form the feedback vector $\boldsymbol{v}$. Figure 5b shows the generalized block

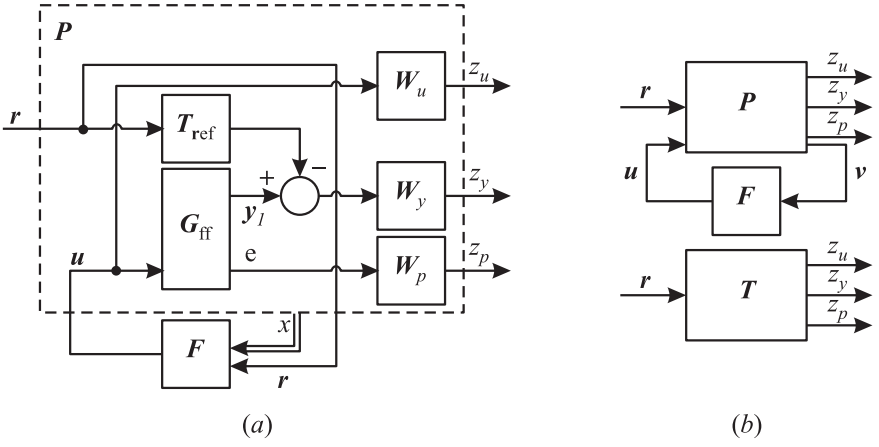

Figure 5 Augmented plant for feedforward design (a) and generalized closed loop (b): $\boldsymbol{u}$ is defined in (5); $\boldsymbol{e}$ in (4); $\boldsymbol{y}_1 = [\mathrm{Nz_{CG}}]$; $\boldsymbol{r} = \mathrm{Nz_{CG\,c}}$; and $\boldsymbol{v} = [x\ r]^{\mathrm{T}}$

$$\begin{bmatrix} \dot{\boldsymbol{x}}(t) \\ \boldsymbol{z}(t) \\ \boldsymbol{x}(t) \\ \boldsymbol{r}(t) \end{bmatrix} = \underbrace{\left[\begin{array}{c|cc} \boldsymbol{A}_{\mathrm{P}} & \boldsymbol{B}_{\mathrm{P}_1} & \boldsymbol{B}_{\mathrm{P}_2} \\ \hline \boldsymbol{C}_{\mathrm{P}_1} & \boldsymbol{D}_{\mathrm{P}_{11}} & \boldsymbol{D}_{\mathrm{P}_{12}} \\ \boldsymbol{I} & \boldsymbol{0} & \boldsymbol{0} \\ \boldsymbol{0} & \boldsymbol{I} & \boldsymbol{0} \end{array}\right]}_{P} \begin{bmatrix} \boldsymbol{x}(t) \\ \boldsymbol{r}(t) \\ \boldsymbol{u}(t) \end{bmatrix}, \tag{8}$$

as well as the lower LFT $\boldsymbol{T} = \mathcal{F}_{\mathrm{l}}(\boldsymbol{P}, \boldsymbol{F})$ with the performance transfer paths from r to z_y, $\boldsymbol{z}_u$, and $\boldsymbol{z}_p$ to be minimized:

$$\left\| \begin{matrix} \boldsymbol{T}_{z_u,r} \\ \boldsymbol{T}_{z_y,r} \\ \boldsymbol{T}_{z_p,r} \end{matrix} \right\|_{\infty} < \gamma. \tag{9}$$

The system matrices $\boldsymbol{A}_P, \ldots, \boldsymbol{D}_{P_{12}}$ in (8) basically correspond to those in [10]; however, they have to be extended to account for the additional system dynamics of $\boldsymbol{W}_p$. Due to the resulting high complexity originating from the state feedback law, a more detailed decomposition of the single performance transfer paths $\boldsymbol{T}_i$ is not considered at this point. Three approaches for solving the $\mathcal{H}_\infty$ optimization problem of (9) in MATLAB are:

(1) building the interconnected structure according to Fig. 5 and using the function hinfsyn with the method setting 'ric.' Using this setting, the full information gain matrix is included in the output argument 'info;'

(2) instead of hinfsyn, also, the function msfsyn can be used. The advantage of this function is that it can be applied to LPV systems determined by a polytopic model; and

(3) formulating the appropriate LMIs according to [10] and using, for example, the LMI solver mincx of LMILAB.

The latter has been shown to be efficient and can be simply inherited for the LPV design case. With the feedback gain matrix $\boldsymbol{F}_{\mathrm{opt}}$ as the primary optimization result of (9), the feedforward controller $\boldsymbol{K}_{\mathrm{ff}}$ is obtained by the lower LFT (Fig. 6):

$$\boldsymbol{K}_{\mathrm{ff}} = \mathcal{F}_{\mathrm{l}}(\boldsymbol{P}_{\mathrm{ff}}, \boldsymbol{F}_{\mathrm{opt}})$$

where $\boldsymbol{P}_{\mathrm{ff}}$ is a modified augmented plant:

$$\boldsymbol{P}_{\mathrm{ff}} = \left[\begin{array}{c|cc} \boldsymbol{A}_P & \boldsymbol{B}_{P_1} & \boldsymbol{B}_{P_2} \\ \hline \boldsymbol{C}_{P_{\mathrm{ff},1}} & \boldsymbol{D}_{P_{\mathrm{ff},11}} & \boldsymbol{D}_{P_{\mathrm{ff},12}} \\ \boldsymbol{I} & \boldsymbol{0} & \boldsymbol{0} \\ \boldsymbol{0} & \boldsymbol{I} & \boldsymbol{0} \end{array}\right]$$

with

$$\boldsymbol{C}_{P_{\mathrm{ff},1}} = \begin{bmatrix} \boldsymbol{EC} & \boldsymbol{0} & \boldsymbol{0} & \boldsymbol{0} & \boldsymbol{0} \\ \boldsymbol{0} & \boldsymbol{0} & \boldsymbol{0} & \boldsymbol{0} & \boldsymbol{0} \end{bmatrix}; \quad \boldsymbol{D}_{P_{\mathrm{ff},11}} = \begin{bmatrix} \boldsymbol{0} \\ \boldsymbol{0} \end{bmatrix}; \quad \boldsymbol{D}_{P_{\mathrm{ff},12}} = \begin{bmatrix} \boldsymbol{ED} \\ \boldsymbol{I} \end{bmatrix};$$

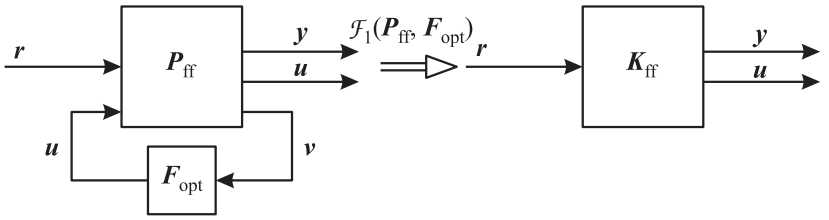

Figure 6 Feedforward controller $\boldsymbol{K}_{\mathrm{ff}}$ obtained by lower LFT from the modified generalized closed loop

and $\boldsymbol{E}$ as a selector matrix, necessary to select those outputs from $\boldsymbol{C}$ and $\boldsymbol{D}$ of the design model (5) utilized as measurements by the feedback controller. The identity matrix $\boldsymbol{I}$ in $\boldsymbol{D}_{P_{\mathrm{ff},12}}$ provides a direct feed-through of the control vector $\boldsymbol{u}$ to the output.

3.2 Reference Model and Performance Weighting Function Definition

To accomplish the required design specifications, an appropriate reference model as well as a correct shape for the performance weighting functions has to be selected.

Reference model $\boldsymbol{T}_{\mathbf{ref}}$: The reference model selected for the model matching problem must, first of all, fulfill the requirements concerning rise time, overshoot, and settling time of the controlled variable $\mathrm{Nz_{CG}}$ to be tracked. Moreover, it is advantageous to incorporate existing actuator dynamics G_{act} and sensor delay G_{sen} in the reference model, since those dynamics represent hard constraints for the attainable tracking response which must not be ignored in the design. Therefore, the reference model T_{ref} consists of three components

$$T_{\mathrm{ref}} = G_{\mathrm{sen}} G_{\mathrm{ref}} G_{\mathrm{act}}$$

where G_{sen} is the first-order Padé approximation with 160-millisecond delay and G_{act} is the linearized model of the slowest actuator, the combined elevator EL_t:

$$G_{\mathrm{sen}} = \frac{s - 12.5}{s + 12.5}\,; \qquad G_{\mathrm{act}} = \frac{7.5}{s^2 + 3.9s + 7.5}\,.$$

The reference transfer function is given by a second-order system:

$$G_{\mathrm{ref}} = \frac{\omega^2}{s^2 + 2\zeta\omega s + \omega^2}$$

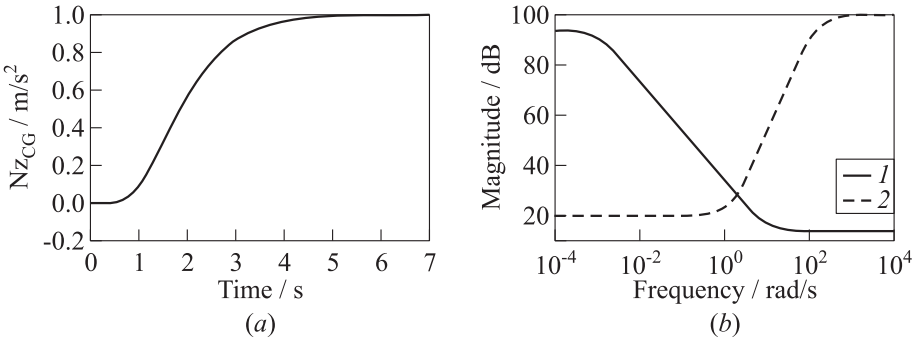

Figure 7 Time response T_{ref} representing an ideal $\mathrm{Nz_{CG}}$ command response (a) and frequency response plot of weighting functions $\boldsymbol{W}_y$ (*1*) and $\boldsymbol{W}_u$ (*2*) (b)

with its parameters set to $\omega = 1.5$ rad/s and $\zeta = 1$. The corresponding time response of the reference model T_{ref} is shown in Fig. 7*a*.

Command tracking $\boldsymbol{W_y}$: For command tracking, the difference between the reference model T_{ref} and the system output to be tracked must be minimized. This can be achieved by a low pass filter of the form

$$\boldsymbol{W}_y = t_{y1}\frac{s + t_{y2}\cdot 10}{s + t_{y2}\cdot 0.001}\,, \tag{10}$$

as shown in Fig. 7*b*, with the corresponding tuning parameters t_{y1} and t_{y2} appropriately set.

Control energy $\boldsymbol{W_u}$: The control energy demanded by the feedforward controller for reference model tracking can be adjusted by high-pass filters of the form:

$$\boldsymbol{W}_u = \begin{bmatrix} t_{u11}\dfrac{(s + t_{u21}\cdot 1)^2}{(s + t_{u21}\cdot 100)^2} & 0 & 0 \\ 0 & t_{u12}\dfrac{(s + t_{u22}\cdot 1)^2}{(s + t_{u22}\cdot 100)^2} & 0 \\ 0 & 0 & t_{u13}\dfrac{(s + t_{u23}\cdot 1)^2}{(s + t_{u23}\cdot 100)^2} \end{bmatrix} \tag{11}$$

with their general shape shown in Fig. 7*b*. The tuning factor t_{u1i} serves to limit the absolute deflections, while t_{u2i} is used to constrain the deflection rates. According to the actuator properties, the tuning factor t_{u2i} is highest for the outmost flap FL_3. Second-order filters are utilized to ensure a sufficiently steep roll-off and, thereby, minimize excitation of the aeroelastic modes by the manoeuvre.

Manoeuvre loads $\boldsymbol{W_p}$: The maximum manoeuvre loads primarily originate from the static content and the first wing bending mode as will be shown below. Thus, static weighting is sufficient for those performance outputs:

$$\boldsymbol{W}_p = \begin{bmatrix} t_{p1} & 0 & 0 \\ 0 & t_{p2} & 0 \\ 0 & 0 & t_{p3} \end{bmatrix}. \tag{12}$$

4 CONTROLLER TUNING

With the design architecture according to subsection 3.1 and the general shape of corresponding weighting functions as defined in subsection 3.2, the subsequent design step is the selection of the tuning factors. This can be carried out either manually or in an automated way as will be presented in the following.

4.1 Manual Tuning

Manually adjusting the factors of the performance weighting functions (10)–(12) is not a trivial task when several design specifications have to be considered at the same time. However, a basic understanding of the design tuning knobs is crucial for a successful control design. Exemplarily, t_{y1} is varied to show the effect on tracking performance and t_{p1} is varied to evaluate the effect of manoeuvre load control. In Fig. 8, the unit step time response of $\boldsymbol{K}_{\text{ff}}$ from r to Nz_{CG}, q_{CG}, and

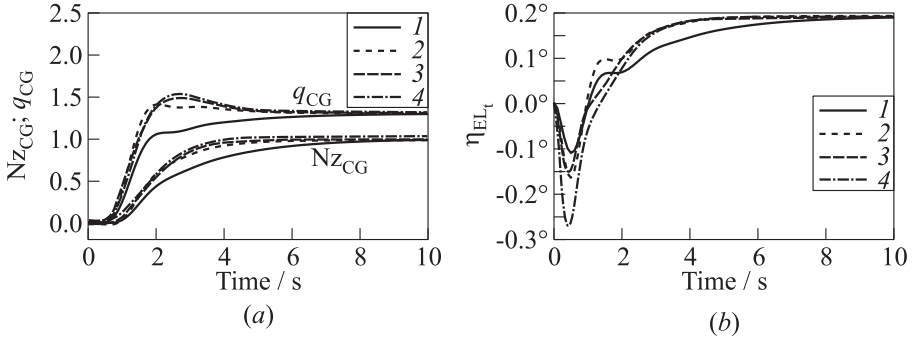

Figure 8 Unit step time response of $\boldsymbol{K}_{\text{ff}}$ from r to Nz_{CG} and q_{CG} for increasing tuning factor t_{y1} (a) and corresponding η_{EL} time response (b): *1* — $t_{y1} = 10^{-2}$; *2* — 10^{-1}; *3* — 10^{0}; and *4* — $t_{y1} = 10^{1}$

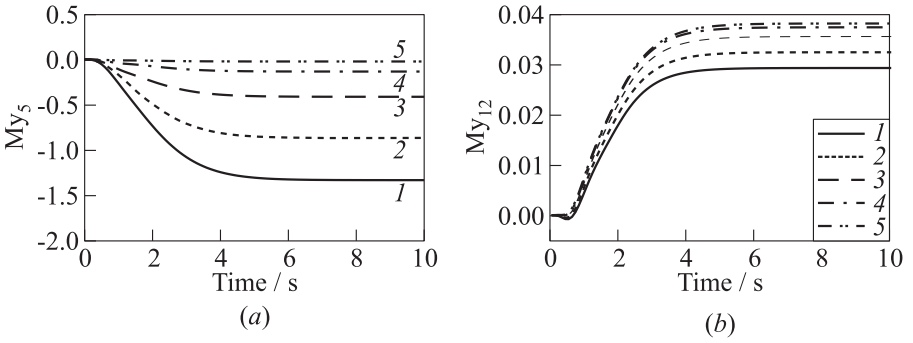

Figure 9 Unit step time response of $\boldsymbol{K}_{\mathrm{ff}}$ from r to My_5 for increasing tuning factor t_{p1} (a) and corresponding My_{12} time response (b): *1* — $t_{p1} = 0.1$; *2* — 0.5; *3* — 1.0; *4* — 2.0; and *5* — $t_{p1} = 10.0$

η_{EL_t} is shown. Therefore, t_{y1} was increased stepwise from $t_{y1} = 10^{-2}$ where $t_{y1} = 10^{0}$ represents an optimized setting. In spite of the high tuning parameter variation, the effect on the tracking performance is moderate. Increasing t_{y1} improves tracking performance and also requires faster control inputs. The effect of increased t_{p1} is presented in Fig. 9. There, manoeuvre loads at the wing root My_5 and at the outer wing My_{12} are compared. Increasing the weighting on one load output typically leads to reduced manoeuvre loads at this and adjacent cut loads; however, this can also cause increased loads at more distant load outputs (waterbed effect). Basically, it has been shown that including the wing bending load outputs My also positively affects the vertical force load outputs Fz. In general, a strong correlation between load outputs and control energy outputs is evident.

4.2 Automated Tuning

In order to accelerate the aforementioned tuning parameter selection, an automated approach is suggested in this subsection. Therefore, several optimization criteria must be formulated which describe the design specifications listed in subsection 2.2 in a mathematical way. The following criteria are based on a reference command step $r = 1.5 \cdot 9.81\ \mathrm{m/s^2}$, which is a typical validation step to investigate maximum control deflections and rates. For the sake of brevity, $y_1(t) = y_{\mathrm{Nz_{CG}}}(t)$ and $y_2(t) = y_{q_{\mathrm{CG}}}(t)$ and the reference response for $\mathrm{Nz_{CG}}$ is y_{ref}:

1. Minimization of the deviation from the $\mathrm{Nz_{CG}}$ reference model time response:

$$c_1 = \sum_{t_{\mathrm{i}}=1}^{5} (y_1(t_i) - y_{\mathrm{ref}}(t_i))^2 \,.$$

2. Limitation of the q_{CG} overshoot:

$$c_2 = \begin{cases} \left(\dfrac{\hat{y}_2}{\overline{y}_2}\right)^2 - 1.3^2\,, & \text{if } \dfrac{\hat{y}_2}{\overline{y}_2} > 1.3\,; \\ 0\,, & \text{otherwise} \end{cases}$$

where $\hat{y}_2$ and $\overline{y}_2$ are the maximum and the stationary value of $y_2(t)$, respectively:

$$\hat{y}_2 = \max_{t<10} y_2(t)\,; \quad \bar{y}_2 = y_2(t=10)\,.$$

3. Limitation of the control energy:

$$c_3 = \begin{cases} \left(\dfrac{\hat{\eta}_i}{\eta_{i\,\max}}\right)^2\,, & \text{if } \dfrac{\hat{\eta}_i}{\eta_{i\,\max}} > 0.95\,; \\ 0\,, & \text{otherwise}\,; \end{cases}$$

$$c_4 = \begin{cases} \left(\dfrac{\hat{\dot{\eta}}_i}{\dot{\eta}_{i\,\max}}\right)^2\,, & \text{if } \dfrac{\hat{\dot{\eta}}_i}{\dot{\eta}_{i\,\max}} > 0.95\,; \\ 0\,, & \text{otherwise} \end{cases}$$

where $\hat{\eta}_i$ and $\hat{\dot{\eta}}_i$ are the maximum deflection and deflection rate of the demanded control signal, respectively:

$$\hat{\eta}_i = \max_{t<10} |\eta_i(t)|\,, \quad \hat{\dot{\eta}}_i = \max_{t<10} |\dot{\eta}_i(t)|$$

while $\eta_{i\,\max}$ and $\dot{\eta}_{i\,\max}$ are the specified actuator properties.

4. Minimization of manoeuvre loads: for manoeuvre loads reduction, a comparative value is necessary. Here, it is obvious to use the loads obtained with the LPV feedback controller $\widehat{\mathrm{My}}_{i\mathrm{fb}}$ mentioned in section 3 for comparison:

$$c_5 = \left(\frac{h_i \widehat{\mathrm{My}}_{i\mathrm{ff}}}{\widehat{\mathrm{My}}_{i\mathrm{fb}}}\right)^2$$

where

$$\widehat{\mathrm{My}}_{i\mathrm{ff}} = \max_{t<10} \mathrm{My}_{i\mathrm{ff}}(t)\,; \quad \widehat{\mathrm{My}}_{i\mathrm{fb}} = \max_{t<10} \mathrm{My}_{i\mathrm{fb}}(t)\,.$$

The factor h_i is a weighting factor indicating the impact of the load output in the optimization. Typically, this factor is set to $1 \le h_5 \le 2$ for the load output at the wing root My_5 and to $0.95 \le h_{9,12} \le 1.2$ for the outer positions My_9 and My_{12}. The primary goal of the optimization is to reduce loads at the wing root without increasing the loads at the outer wing.

All these criteria are summed up and form the final cost function to minimize:

$$\min_{t_{y1},t_{u11},t_{u12},t_{u13},t_{p1},t_{p2},t_{p3}} = \sum_{i=1}^{5} c_i \,. \tag{13}$$

The factors t_{y2}, t_{u21}, t_{u22}, and t_{u23} are not included in the optimization. Those are determined *a priori* and kept constant during the optimization. In order to solve the optimization problem (13), different optimization tools can be applied at this stage. Here, a genetic algorithm is utilized which is provided by the the optimization toolbox in MATLAB. The theoretical background on genetic algorithms in connection to control applications can be found in [17, 18]. A further practical approach is given in [19].

5 LINEAR PARAMETER-VARYING DESIGN VERSUS *A POSTERIORI* SCHEDULING

Up to now, the nominal design case for the feedforward controller was considered. Now, also the parameter-varying case will be investigated, i. e., the dynamics of the linear design plant is parameter dependent $\boldsymbol{G}_{\text{ff}} = \boldsymbol{G}_{\text{ff}}(\rho(t))$ where $\rho(t)$ represents the flight parameters q and Ma as well as the fuel mass parameter f. The fuel mass parameter is also taken into consideration, since the obtained robust performance over the entire fuel mass parameter range was not satisfactory. The parameter dependency of the plant also means that the augmented plant according to (8) is parameter dependent $\boldsymbol{P} = \boldsymbol{P}(\rho(t))$, with the appropriate weighting functions $\boldsymbol{W}_u$, $\boldsymbol{W}_y$, and $\boldsymbol{W}_p$ determined as shown in subsection 4.2. In order to account for the parameter dependency, two onsets were considered:

(1) LPV design approach including the vertex plants in the LMI optimization; and

(2) *A posteriori* scheduling by linear interpolation.

5.1 Linear Parameter-Varying Design

Due to the remaining complexity of the design model $\boldsymbol{G}_{\text{ff}}$ and the strong variations of the system dynamics with varying scheduling parameters, the considered flight envelope has to be decomposed into smaller regions. Otherwise, no feasible solution can be obtained. Also, considering the fuel mass as a third scheduling parameter leads to infeasible solutions. Therefore, for demonstration purposes, the reduced parameter space $8\,000 \leq q \leq 17\,238$, $0.82 \leq \text{Ma} \leq 0.85$, and a fixed fuel mass $f = 90\%$ was chosen. In the LMI optimization, the models at the corners of the polytopic subspace were used:

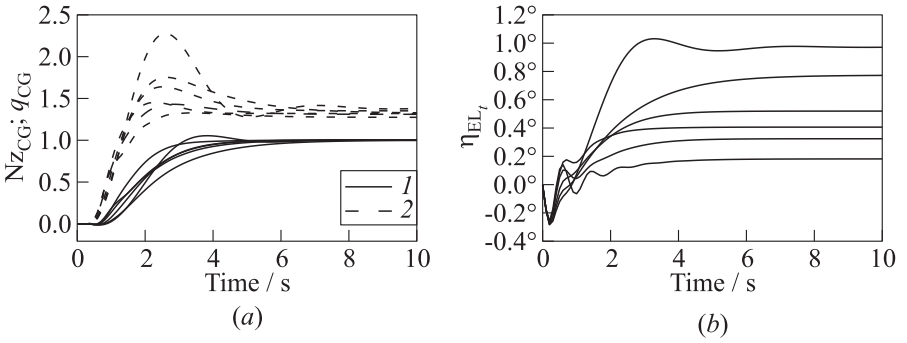

Figure 10 Unit step response of LPV $\boldsymbol{K}_{\mathrm{ff},i}$ from r to $\mathrm{Nz_{CG}}$ (*1*) and q_{CG} (*2*) for varying q and Ma (*a*) and corresponding η_{EL_t} time response (*b*)

$$\begin{aligned}
\boldsymbol{P}_1 &= \boldsymbol{P}_1(q = 8\,000, \mathrm{Ma} = 0.82, f = 90)\,; \\
\boldsymbol{P}_2 &= \boldsymbol{P}_2(q = 8\,000, \mathrm{Ma} = 0.85, f = 90)\,; \\
\boldsymbol{P}_3 &= \boldsymbol{P}_3(q = 17\,238, \mathrm{Ma} = 0.82, f = 90)\,; \\
\boldsymbol{P}_4 &= \boldsymbol{P}_4(q = 17\,238, \mathrm{Ma} = 0.85, f = 90)\,.
\end{aligned}$$

The weighting functions and reference models, however, are equivalent for all augmented plants $\boldsymbol{P}_i$. The LMI optimization provides the feedback matrix $\boldsymbol{F}$, which can be connected to every modified augmented plant $\boldsymbol{P}_{\mathrm{ff},i}$ within the considered polytopic subspace. A simple way of validation is to plot the unit step response from r to the outputs $\boldsymbol{y}$ and $\boldsymbol{u}$ for the obtained feedforward controllers $\boldsymbol{K}_{\mathrm{ff},i}$. Exemplarily, this is shown in Fig. 10 for the corner parameters used in the design and two parameter combinations in the middle. In Fig. 10*a*, the $\mathrm{Nz_{CG}}$ and q_{CG} response and in Fig. 10*b*, the control signal η_{EL_t} are shown. It turns out that the command response of four controllers is satisfactory, whereas in one case, the damping is too low and in another, the response is to slow. Both outliers are the controllers at extremal parameter cases. The control signal shows in any case all-pass behavior; in one case, a comparatively high-frequency signal is apparent.

5.2 *A Posteriori* Scheduling

The *a posteriori* scheduling approach is composed of the following design steps:

(1) automated weighting factor optimization according to subsection 4.2 on a rough gridding comprising the flight envelope of interest;

(2) validation of the obtained grid point controllers;

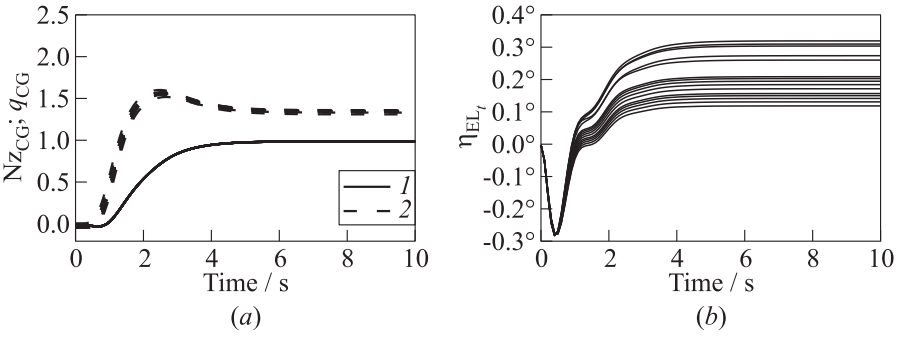

Figure 11 Unit step response of *a posteriori* scheduled $\boldsymbol{K}_{\mathrm{ff},i}$ from r to $\mathrm{Nz_{CG}}$ (*1*) and q_{CG} (*2*) for $0.82 \leq \mathrm{Ma} \leq 0.835$ and $q = 9\,000$ (*a*) and corresponding η_{EL_t} time response (*b*)

(3) design of intermediate grid point controllers using weighting functions obtained by linear interpolation of the weighting functions from the rough gridding; and

(4) element-wise linear interpolation of the system matrices $\boldsymbol{A}$, $\boldsymbol{B}$, $\boldsymbol{C}$, and $\boldsymbol{D}$ from the finely gridded $\boldsymbol{K}_{\mathrm{ff},i}$.

In Fig. 11*a*, the $\mathrm{Nz_{CG}}$ and q_{CG} responses of the linearly interpolated controllers $\boldsymbol{K}_{\mathrm{ff},i}$ to a unit reference step are shown exemplarily for the parameters $q = 9\,000$, $f = 90\%$, and $0.82 \leq \mathrm{Ma} \leq 0.835$. The response hardly changes with varying Ma number. In Fig. 11*b*, the corresponding η_{EL_t} time response is plotted. Strong variations of the control signal for only moderate changes in Ma number become evident. The validation results presented in section 6 are obtained using the *a posteriori* scheduling approach.

6 VALIDATION RESULTS

In this section, the obtained parameter-dependent feedforward controller $\boldsymbol{K}_{\mathrm{ff}}(\mathrm{Ma}, q, f)$ is validated in order to assess the performance improvement obtained by this prefilter. Before considering the obtained results, two points have to be recalled:

(1) the designed feedforward controller $\boldsymbol{K}_{\mathrm{ff}}$ is validated together with a preliminary LPV feedback controller $\boldsymbol{K}_{\mathrm{fb}}$, forming together a 2DOF control architecture according to Fig. 4; and

(2) the validation model contains 19 aeroelastic modes, the actuator dynamics is given by a nonlinear model (depending on the dynamic pressure q), the

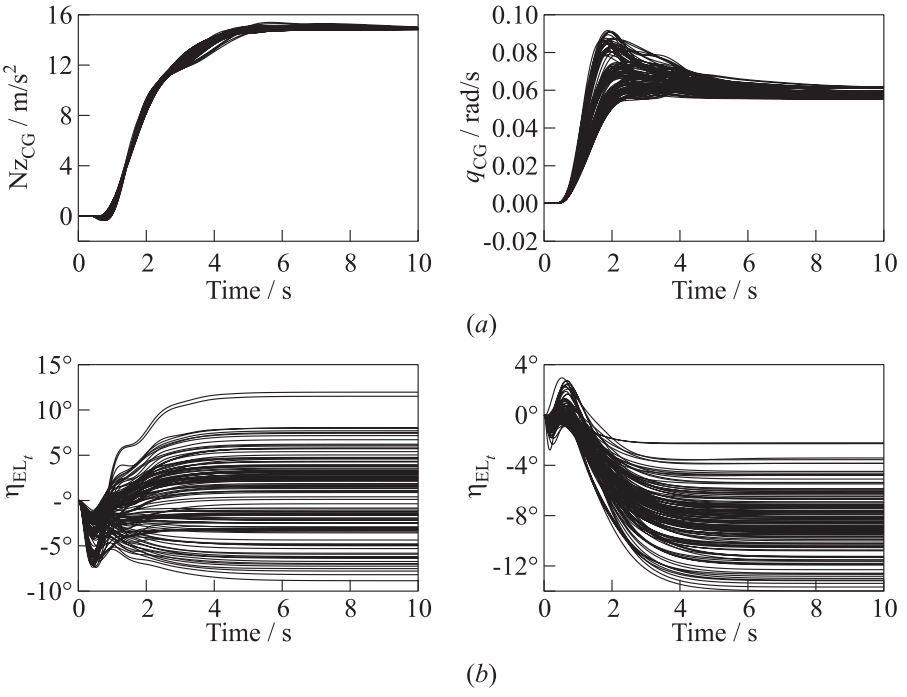

Figure 12 Time responses Nz_{CG} (a) and η_{EL_t} (b) to $r = 1.5g$ reference command for validation models spanning the entire parameter range according to (7) chosen from the envelope (left column) and corresponding q_{CG} (a) and η_{EL_t} (b) time responses (right column)

sensor dynamics is modeled by Butterworth filters and second-order Padé approximations of the time delays, and control inputs are limited by saturation and rate limits.

The following validation plots show the system response to an $r = 1.5g$ reference command where $g = 9.81$ m/s^2 is the gravity constant. Such a high reference value leads, on the one hand, to an actuator operation far off its stationary linearization point and, on the other hand, almost reaches or exceeds saturation and rate limits. Moreover, the maximum manoeuvre loads can be directly determined. The validation models considered here describe a representative set of grid point models taken equally distributed from the envelope according to (7). In Fig. 12a, the Nz_{CG} and q_{CG} responses are shown. The Nz_{CG} response has similar characteristics independent of the parameter case and fulfills basically the requirements concerning rise time and overshoot. A slightly rippled response after $t = 3.5$ s is noticeable for some of the validation models. This

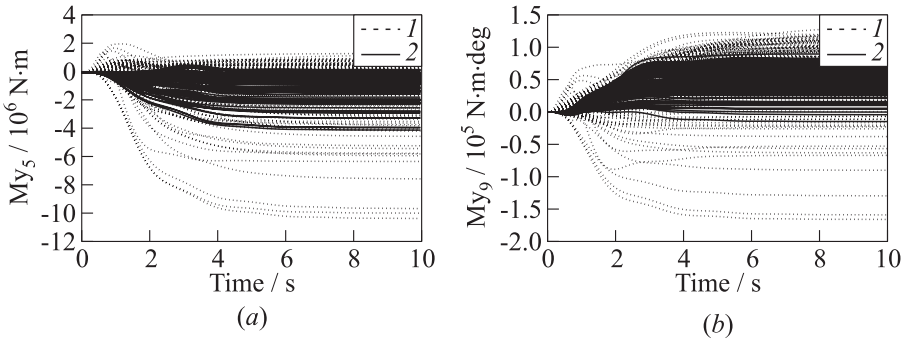

Figure 13 Time response My_5 comparison of $\boldsymbol{K}_{\mathrm{fb}}$ (*1*) and 2DOF (*2*) to $r = 1.5g$ m/s^2 reference command for validation models spanning the entire parameter range according to (7) chosen from the envelope (*a*) and corresponding My_9 time response (*b*)

can be explained by a comparatively higher deviation of the linearized actuator model used for design from the nonlinear model. This deviation is only moderately compensated by the feedback controller and, therefore, visible in the time response. The rise time of the q_{CG} response is slightly faster in connection with the corresponding overshoot. The upper limit of 30 percent overshoot is slightly exceeded in only a few cases. In Fig. 12*b*, the demanded control signals of $\boldsymbol{K}_{\mathrm{ff}}$ are shown for the combined elevator EL_t (left) and the combined inner flap FL_{12} (right). It turns out that in both cases, the control signal characteristics are similar within the first second independent of the parameter vector. Afterwards, a broad spreading is visible, indicating the strong variations in low-frequency system dynamics. The maximum deflections are well below the deflection limits of the actuators which are:

$$-30^\circ \le \eta_{\mathrm{EL}_t} \le 15^\circ\,; \quad -25^\circ \le \eta_{\mathrm{FL}_{12}} \le 25^\circ\,; \quad -25^\circ \le \eta_{\mathrm{FL}_3} \le 25^\circ\,.$$

This is especially necessary for FL_{12}, which is mainly used for the roll manoeuvre. However, only additional tests can ensure that this actuator does not exceed the deflection limits in extremal coordinated turn manoeuvres. The deflection of FL_3 is slightly higher but still below the maximum deflection limits. Time plots of the maximum deflection rates are not presented here; however, validation of those have shown that the given rate limits are not exceeded. In Fig. 13, a comparison of the manoeuvre loads My_5 and My_9 is shown for the closed loop with $\boldsymbol{K}_{\mathrm{fb}}$ only (*1*) and for the 2DOF concept (*2*). A significant reduction of incremental loads is visible for both outputs, which underlines the effectiveness of the chosen design approach.

In a detailed analysis of structural loads, not only the manoeuvre loads are of interest but also dynamic loads caused by turbulence gusts. Alleviation of turbulence gust loads is not addressed with the feedforward concept presented here.

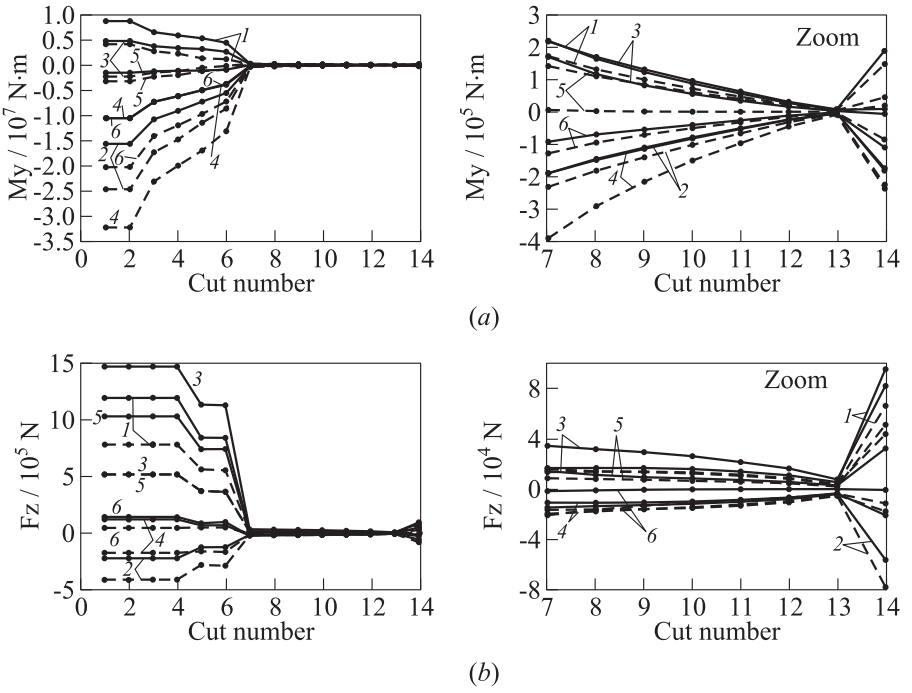

Figure 14 Comparison of maximum and minimum cut moments My (a) and Fz (b) over all cut positions along the wing and over the flight envelope according to (7) for various validation cases: *1* — G_d; *2* — G_u; *3* — $M_p\boldsymbol{K}_{\text{fb}}$; *4* — $M_n\boldsymbol{K}_{\text{fb}}$; *5* — $M_{p2\text{DOF}}$; and *6* — $M_{n2\text{DOF}}$. Solid curves refer to maximum and dashed to minimum loads

However, a comparison of the maximum loads caused by manoeuvre and gust gives information which of those external excitations determines the structural sizing loads. Those, in turn, are used for a resizing process.

In Fig. 14, a comparison of maximum and minimum loads over all cut positions along the wing and over the flight envelope according to (7) essentially for three validation cases are shown:

(1) up and down gust (G_u and G_d);

(2) $+1.5g$ and $-1.0g$ manoeuvre (M_p and M_n) using $\boldsymbol{K}_{\text{fb}}$ controller only; and

(3) $+1.5g$ and $-1.0g$ manoeuvre using 2DOF controller.

The loads caused by up and down gust are determined using a standardized 1-cos gust [20] input to the global vertical gust input of the system. The 1-cos gust parameters, integral scale length, and maximum vertical gust velocity, are varied in order to detect their worst case combination causing the maximum

loads. When considering Fig. 14*a*, it turns out that the absolute maximum bending moments My_i are caused by manoeuvres using $\boldsymbol{K}_{\mathrm{fb}}$ controller only. On the contrary, the absolute maximum gust loads are approximately 25% lower.

The additional feedforward controller $\boldsymbol{K}_{\mathrm{ff}}$ reduces manoeuvre loads up to 35% and renders the gust loads the new sizing loads. A similar characteristic is given for the vertical force load outputs Fz_i. Again, the 2DOF controller reduces the cut forces significantly which makes the gust loads sizing.

7 CONCLUDING REMARKS

In this paper, an $\mathcal{H}_\infty$ full information feedforward design approach was utilized to design a prefilter for longitudinal motion control of a large flexible BWB aircraft. An already existing onset was extended in order to fulfill specifications concerning command tracking and limited control energy but also the stringent requirement of reduced manoeuvre loads. An adequate design architecture within the standard $\mathcal{H}_\infty$ framework and appropriate performance weighting was presented. The controller tuning process was outlined for manual and automated tuning in order to obtain high-performance feedforward controllers. The considered, large flight envelope, and the strong variation of system dynamics with changes in flight parameters make an extension to an LPV or scheduled design inevitable. In this regard, two onsets are presented, both applicable for the given problem setting. Finally, the obtained scheduled feedforward control laws were validated together with an already existing LPV feedback controller over the considered flight envelope on a high-order nonlinear model. It turned out that the requirements concerning command shaping under consideration of limited control energy are satisfied. At the same time, manoeuvre loads are significantly reduced over the entire wing. This changed the loads caused by turbulence gust into sizing loads. These results and the fact that the design can be used for a large parameter space make the presented approach an interesting and powerful design methodology for flexible aircraft control.

ACKNOWLEDGMENTS

This work was financially supported by the European Union Framework Programme 7 under the FP7 project No. 213321 [11].

REFERENCES

1. Hanel, M. 2001. *Robust integrated flight and aeroelastic control system design for a large transport aircraft*. VDI-Verlag. No. 866.
2. Kron, A., J. de Lafontaine, and D. Alazard. 2003. Robust 2-DOF H-infinity controller for highly flexible aircraft: Design methodology and numerical results. *Can. Aeronautics Space J.* 49:19–29.

3. Jeanneau, M., J. Lamolie, G. Puyou, and N. Aversa. 2005. Awiators design of multi-objectives control laws. *IFAC*.
4. Westermayer, C., A. Schirrer, M. Hemedi, M. Kozek, and A. Wildschek. 2009. Robust $\mathcal{H}_\infty$ flight and load control of a flexible aircraft using a 2DOF multi-objective design. *2009 CACS Automatic Control Conference (International) Proceedings*.
5. Wildschek, A., R. Maier, M. Hromčík, T. Haniš, A. Schirrer, M. Kozek, Ch. Westermayer, and M. Hemedi. 2009. Hybrid controller for gust load alleviation and ride comfort improvement using direct lift control flaps. *3rd EUCASS Proceedings*.
6. Torralba, J., G. Puyou, and F. Demourant. 2009. Self-scheduling multiobjective control law design for a flexible aircraft. *AIAA Guidance, Navidation, and Control Conference*. Chicago, USA.
7. Schirrer, A., C. Westermayer, M. Hemedi, and M. Kozek. 2011. Multi-model convex design of a scheduled lateral feedforward control law for a large flexible BWB aircraft. *18th IFAC World Congress Preprints*. Milano, Italy. 2126–31.
8. Schirrer, A., C. Westermayer, M. Hemedi, and M. Kozek. 2011. Robust convex lateral feedback control synthesis for a BWB aircraft. *18th IFAC World Congress Preprints*. Milano, Italy. 7262–67.
9. Westermayer, C., A. Schirrer, M. Hemedi, and M. Kozek. 2010. Linear parameter-varying control of a large blended wing body flexible aircraft. *18th IFAC Symposium on Automatic Control in Aerospace*. Nara, Japan.
10. Prempain, E., and I. Postlethwaite. 2001. Feedforward control: A full-information approach. *Automatica* 37:17–28.
11. ACFA 2020 Consortium. 2011. Active control of flexible 2020 aircraft (ACFA 2020), EU FP7. Project No. 213321. URL: http://www.acfa2020.eu. (Retrieved: January 31, 2011.)
12. Stroscher, F., Ö. Petersson, and M. Leitner. 2010. Structural optimization framework for aircraft subject to transient maneuver and gust loads. *13th AIAA/ISSMO Multidisciplinary Analysis Optimization Conference Proceedings*. Fort Worth, Texas.
13. Stroscher, F., Ö. Petersson, and M. Leitner. 2010. Aircraft structural optimization subject to flight loads — application to a wide body commercial aircraft configuration. *EASN Workshop (International) on Aerostructures*.
14. Prempain, E., and B. Bergeon. 1998. A multivariable two-degree-of-freedom control methodology. *Automatica* 34(12):1601–6.
15. Prempain, E., and I. Postlethwaite. 2008. A feedforward control synthesis approach for LPV systems. *American Control Conference Proceedings*. 3589–94.
16. Skogestad, S., and I. Postlethwaite. 1996. *Multivariable feedback control analysis and design*. John Wiley & Sons.
17. Fleming, P. J., and R. C. Purshouse. 2001. Genetic algorithms in control systems engineering. *12th IFAC World Congress Proceedings*. 383–90.
18. Fleming, P. J., and R. C. Purshouse. 2002. Evolutionary algorithms in control systems engineering: A survey. *Control Eng. Practice* 10:1223–41.
19. Schirrer, A., C. Westermayer, M. Hemedi, and M. Kozek. 2010. Robust $\mathcal{H}_\infty$ control design parameter optimization via genetic algorithm for lateral control of a BWB type aircraft. *IFAC Workshop on Intelligent Control Systems*. Sinaia, Romania.
20. Hoblit, F. M. 1988. *Gust loads on aircraft: Concepts and applications*. New York: American Institute of Aeronautics and Astronautics.